Femtosecond Laser Damage Threshold and Nonlinear Characterization in Bulk Transparent SiC Materials

G. Logan DesAutels[1], Chris Brewer[2], Mark Walker4, Shane Juhl[2], Marc Finet[1], Scott Ristich[1], Matt Whitaker[1], Peter Powers[3]

[1]AT&T Government Solutions, Dayton, OH 45433
[2]Air Force Research Laboratory, Materials and Manufacturing Directorate, WPAFB, OH 45433
[3]University of Dayton, Dayton, OH 45469
[4]General Dynamics Information Tech., Dayton, OH 45431

Abstract – Semi-insulating and conducting SiC crystalline transparent substrates were studied after being processed by femtosecond laser radiation (780nm at 160fs). Z-scan and damage threshold experiments were performed on both SiC bulk materials to determine each samples' nonlinear and threshold parameters. "Damage" in this text refers to an index of refraction modification as observed visually under an optical microscope. In addition, a study was performed to understand the damage threshold as a function of numerical aperture. Presented here for the first time, to the best of our knowledge, is the damage threshold, nonlinear index of refraction, and nonlinear absorption measured values.

1. Introduction

Femtosecond (fs) lasers have become a very important tool for micromachining and fabrication of photonic devices. Their unique ability of inducing permanent index changes into just about any transparent material is due to fast focusing conditions, resulting in very high intensity causing nonlinear multi-photon absorption. Former research has theorized that the ultra-fast pulse is too short to interact at the molecular level, and instead interacts at the atomic electronic level [1]. Here the fs pulse displaces electrons permanently and/or causes lattice changes resulting in a modification to the index of refraction [2]. The modification to the index is localized to a very small volume depending on the NA and energy used. These index alterations can be on the surface or in most cases subsurface to the bulk material.

SiC is an attractive alternative material for a variety of semiconductor devices where silicon (Si) lacks the environmental resistance that carbon furnishes when combined to Si [3]. These areas where SiC devices can be used include high-power high-voltage switching applications, high temperature electronics, and avionics where it is desired to keep

Nonlinear Frequency Generation and Conversion: Materials, Devices, and Applications VII, edited by Peter E. Powers,
Proc. of SPIE Vol. 6875, 68751M, (2008) · 0277-786X/08/$18 · doi: 10.1117/12.765560

sensitive Si-based electronics away from extreme environments onboard aircraft [3]. However, micro-machining SiC is problematic due to its ability to resist almost any type of etching processes. Examples of the common etching processes are: wet chemical etching, deep reactive ion etching (DRIE), and reactive ion etching (RIE) [4]. For these reasons, it is of some interest to study the laser processing and material characteristics of SiC to provide future alternative methods of micromachining this unique material.

Our method of morphing a circular beam into a high aspect ratio elliptical beam uses an anamorphic lens. The anamorphic lens provides accurate micro-machined lines in the absence of any self-focusing from the use of a highly elliptical beam [5]. The idea/theory is that a large NA in combination with an elliptical beam will decrease the chances of any self-focusing occurring within the bulk of the sample. Self-focusing filamentation will spoil the micro-machined features, which will result in unpredictable/undesired micro-machined features. The gratings produced with the anamorphic lens resist any nonlinear self-focusing attributes, and results in "clean" accurate gratings that closely resemble the geometrical profile.

The anamorphic lens transforms the ultrafast (UF) laser pulse from a 5.5mm round Gaussian fluence distribution to a 2.5µm by 190µm line shape. The SiC samples were laser processed using an automated xyz stage in a direct write configuration. The samples were irradiated with a single laser pulse by use of a chopper wheel and high speed shutter combination. The fs laser pulse was generated using a Clark-MXR CPA-2010 laser system, with a wavelength of 780nm, a pulse width of 150-200fs, $M^2 = 1.55$ and a maximum energy of 1mJ/pulse. Typical pulse energies used in this work were in the 10µJ to 30µJ range.

In this work we report semi-insulating and conducting SiC bulk material linear and nonlinear optical properties, as well as bulk damage threshold (DT) measurements as a function of numerical aperture, NA, (under tight focusing conditions). The linear SiC material properties were measured using UV-Vis spectrometer, which determine the linear transmission and bandgap of the substrate. The 3rd order nonlinear properties are revealed using the Z-scan technique, which present

the nonlinear absorption (β) and the nonlinear index of refraction (n_2). The laser processed portions of the samples were also investigated using optical microscope imagery, and atomic force microscopy (AFM). Finally, all experiments were first calibrated using a fused silica (FS) sample and compared to referenced experimental data to validate our results.

2. Experimental Setups

The DT and Z-scan experiments were completed using a single laser source split into multiple paths. Figure 1 below illustrates the experimental setups.

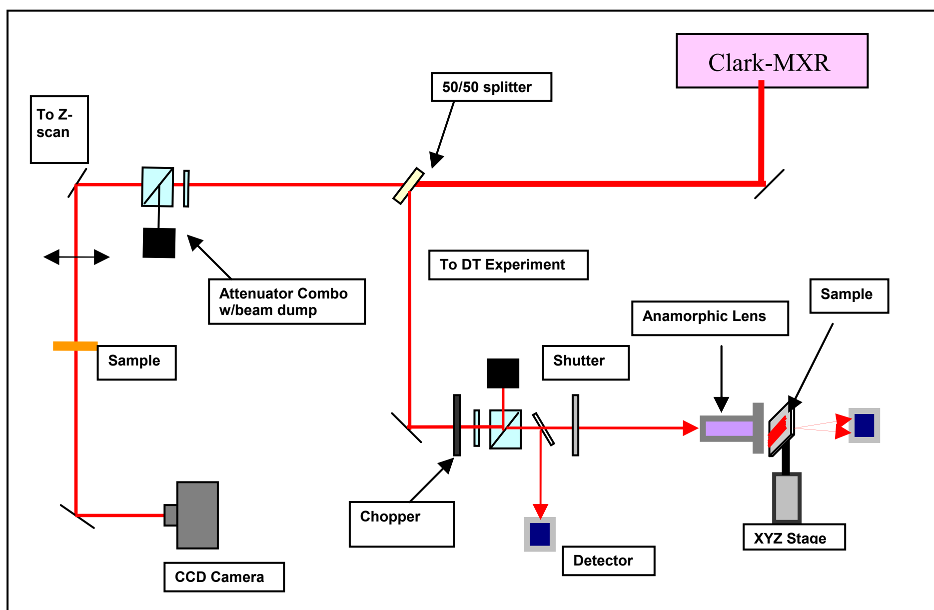

Figure 1 Optical setups for the damage threshold and Z-scan experiments.

Figure 1 gives the experimental setups for both the DT and Z-scan experiments. The Clark-MXR femtosecond laser system is split into multiple beam paths for different tests; a 100µJ portion of that is split for the DT and Z-scan studies. In each experiment line there is a polarizer beam splitter and ½ wave plate combo used to attenuate the beams. The Z-scan uses a 750mm lens to provide a large Rayleigh range, Z_R, and to keep the fluence below the damage threshold. The DT experiment uses the anamorphic lens to morph the 5.5mm circular beam into a 2.5µm x 190µm line distribution as described in the Introduction section.

The Z-scan line uses a CCD camera (DALSA 1M15) to sense the transmitted beam, and the closed aperture is added synthetically, via software image processing. The synthetic aperture types (round or other shapes), range of the Z-scan, and camera calibration are all set before each scan. The experiment uses a large CCD array (typically about twice the beam diameter after focus) and synthetic apertures have allowed ease in alignment of the beam down the Z-scan line. In addition, the software can record an average of beam profiles (intensity) at each Z-location, and then save those images for further analyses.

The DT line uses input and output photodiodes to measure the incident pulse energy verses the transmitted energy through the sample. Each photodiode is calibrated using a pyroelectric Joule meter (traceable to National Institute of Standards). The DT line also has a chopper wheel and a high speed shutter which together work automatically control the number of pulses to the sample. Finally, the sample is held on a xyz automatic stage controlled with ± 1μm accuracy. The entire illumination collection procedure is automated. This configuration, shown in Figure 1, allows for the Z-scan and DT experiments to run simultaneously, but the beams delivered at each experiment are separately characterized for completeness.

3. SiC Characteristics

The SiC samples tested are two types shown in Table 1 below.

Table 1: SiC sample characteristics for semi-insulating and conducting types. Semi-insulating SiC samples are supplied by Intrinsic Corp, and the conducting SiC samples are supplied by Cree Corp.

Sample	Orientation	Dopant	Dopant Concentration (cm^{-3})	Resistivity (Ω·cm)	Thickness (μm)	Face	N or P Type
SiC semi-insulating	c-plane, 6H 0° on axis	Undoped	$\sim 1x10^{15}$	$3x10^{7}$	340	Si	---
SiC conducting	c-plane, 6H 0° on axis	Nitrogen	$\sim 2.5x10^{17}$	0.05	220	Si	N

Each sample in Table 1 was perpendicularly oriented on the c-plane with the vertically polarized circular and anamorphic beams. The nitrogen dopant amounts (~1 part per million) in the conducting sample are so small they can be ignored for this study. The thickness differences between the samples can also be ignored since these are surface studies. The lab/laser conditions are identical. Once the lenses were aligned and characterized each sample was simply inserted

at the same location. The samples have the same dimensions therefore the identical sample mount/position was employed. The tests were run back to back so the laboratory environmental conditions were indistinguishable. Thus, the conductivity/resistivity is the only variable between the two samples.

4. Threshold Measurements

The damage threshold in this text refers to substrate modification observed under an optical microscope using transmission or reflection. The DT values are an important quantity to report for future laser processing of SiC bulk materials. The DT is measured in J/cm^2 for a low numerical aperture (NA) and a high NA, and determines the minimum energy distribution to induce an observable change into the SiC material. The fluence distribution in the beam focus is well-designed as an elliptical and/or circular Gaussian with spot size along each principal axis given by [6],

$$w_{o\,x,y} = \frac{\lambda \cdot f_{x,y} \cdot {M_{x,y}}^2}{\pi \cdot w_z}, \qquad \text{Equation 1}$$

where f is the focal length, λ is the wavelength, M^2 is a measured quantity that is used to characterize the deviation from diffraction limited focusing (M^2 of 1 represents the diffraction limit, and real beams have $M^2 > 1$), and w_z is the spot radius propagating from the laser and is given below,

$$w_z = w_{ox,y} \cdot \sqrt{1 + \left(\frac{Z}{Z_R}\right)^2}, \qquad \text{Equation 2}$$

where Z is the propagation distance from the laser source to the test bed, w_o is the beam spot size, and Z_R is the Rayleigh range. The peak fluence can be determined using

$$F_o = \frac{2 \cdot E}{\pi \cdot w_{ox} \cdot w_{oy}}, \qquad \text{Equation 3}$$

where E is the input energy. The above equations were used for each axis for the elliptical beam formed by the anamorphic lens system, which produced a high NA beam. Figure 2 and Table 2 then gives the damage threshold results for FS, semi-insulating and conducting SiC.

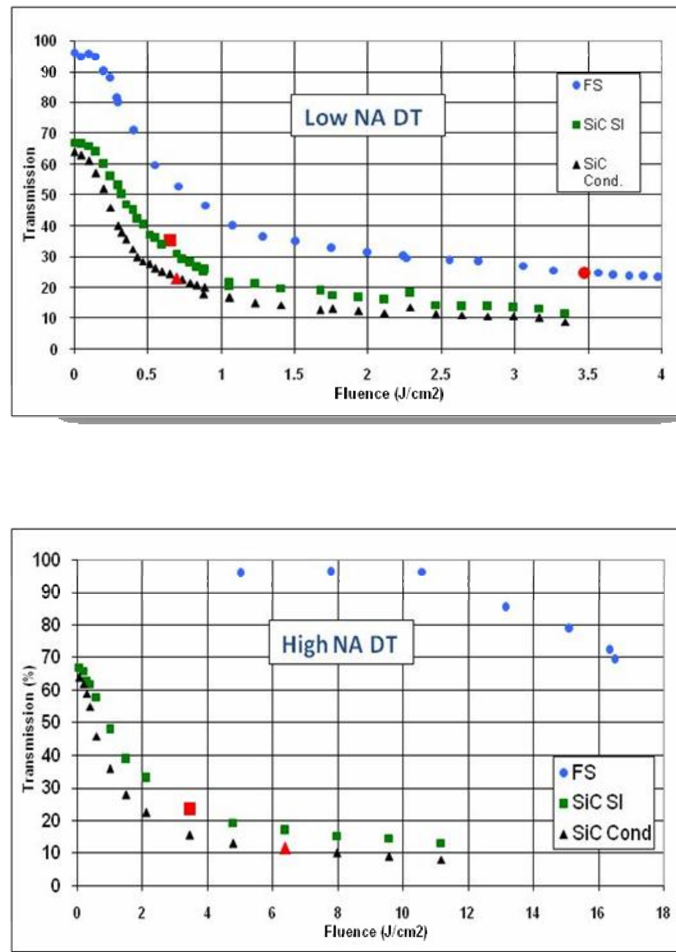

Figure 2 On Top is a plot of the damage threshold (DT) for SiC semi-insulating (SI), SiC conducting, and Fused Silica (FS) using a spherical 125mm lens (NA = 0.022) for 780nm at 160fs. FS is our base-line sample, which is used to calibrate our DT experiments. FS has a DT that is well known to be ~3.0-4.0 J/cm^2 as referenced [7]. On Bottom is the high NA DT plot of SiC semi-insulating, SiC conducting, and FS using an anamorphic lens (NAx = 0.0035 in x and NAy = 0.256 in y) for 780nm at 160fs. The larger red data points represent where the visible damage begins.

These DT results greatly depend on NA as shown in Schaffer-Mazur [5] for tight focusing conditions. In the top chart in Figure 2, the low NA DT data was recorded using a 125mm lens (NA = 0.022). To show the dependence of NA, as Schaffer-Mazur, we employed our anamorphic lens and repeated the high NA (0.256 in y-direction) DT plot shown in the bottom chart in Figure 2. Each DT experiment was done using 780nm at 160fs.

The low and high NA DT results are tabulated in Table 2 below.

Table 2: DT measured results for two lenses: 125mm focal and the anamorphic lens (High NA); using 780nm at 160fs.

Sample	**Low NA DT (J/cm^2)**	**High NA DT (J/cm^2)**	**Bandgap (eV)**
FS	3.7	~20 to 40	9.0 [8]
SiC semi-insulating	0.6	3.5	3.14 [9,10] and Figure 4
SiC conducting	0.65	6.4	3.14 [9,10] and Figure 4

As shown in Table 2 the use of a high NA focusing geometry increases the DT, as inspected under an optical microscope, by a factor of 6 to 10 times from the spherical 125mm lens. The FS sample did not reach a DT for the high NA experiment, and it is predicted that 100μJ (for a fluence of ~30 J/cm^2) or more is needed to create a 2.5μm X 190μm line on or below the surface.

5. Z-scan Study

The nonlinear properties, nonlinear index of refraction (n_2) and nonlinear absorption (β), of SiC semi-insulating and SiC conducting were also investigated. In calculating the nonlinear parameters two approximations are applied to reduce the computation speed and complexity. One is a thin sample approximation where the sample thickness >> Z_R, and the second is the weak nonlinear approximation that assumes the nonlinear process is small [11]. The calculated n_2 data is done using the peak to valley of the closed aperture trend defined by [12]

$$n_2 = \frac{\Delta\Phi_o}{kL} \cdot \frac{1}{I_o}, \qquad \text{Equation 4}$$

where $\Delta\Phi_o$ is the on-axis phase shift at the focus, k is the wave number, L is the length of the sample and I(z,E) is the intensity as a function of z-position and energy for a Secant pulse given by [12]

$$I(z,E) = \frac{2E \cdot \ln\left(1+\sqrt{2}\right)}{\Delta t \cdot \pi \cdot w_o^{\,2}}, \qquad \text{Equation 5}$$

where Δt is the pulse width, w_x and w_y are the spot radii of the beam in x and y directions. As stated above, $\Delta\Phi_o$ is the on-axis phase shift, ΔΦ, which can be experimentally determined by examining the peak-valley transmission change in the closed aperture case using [12]

$$\left|\Delta\Phi_o\right| = \frac{\Delta T_{pv}}{(0.406)(1-S)^{0.25}}, \qquad \text{Equation 6}$$

where S is the linear transmittance aperture (S-Parameter) and defined by [12]

$$S = 1 - \exp\left(-2\frac{r_a^{\,2}}{w_a^{\,2}}\right). \qquad \text{Equation 7}$$

Here, r_a is the radius of the closed aperture and w_a is the radius of the laser beam at the location of the closed aperture. Equation 4 can then be used to recover the n_2 value of the sample under test.

We will not go into much detail with the fit data simply to keep this paper simplified, rather we direct the reader to reference [13], which describes precisely how to apply the theory and equations to any mathematical software such as Mathcad, Matlab, etc. The normalized open aperture signal is fitted to [13]

$$Tx(z,\beta,E) := \frac{1}{2\cdot qo(z,\beta,E)}\cdot\int_{-\infty}^{\infty} \ln\left(1 + qo(z,\beta,E)\cdot \mathrm{sech}\,(x)^2\right) dx, \qquad \text{Equation 8}$$

where q_o is defined by [13]

$$qo(z,\beta,E) := \beta\cdot I(z,E)\cdot L, \qquad \text{Equation 9}$$

This work utilizes the open and closed fits to average the noise in the data. The peak-valley of the closed data fit is used to calculate the on-axis phase shift.

For the FS and SiC data a synthetic closed aperture of 0.55mm, and open aperture of 5mm, repetition rate of 41Hz (with assistance from a chopper wheel), an S-parameter set to 15%, and energy ranging from 2μJ to 4uJ. Multiple energies were used to ensure consistent nonlinear measurements. The beam was characterized before the experiments by

performing an M^2 measurement, the pulse width using a Clark-MXR AC 150 Auto-correlator, and profiling the beam with a Cohu CCD camera. The beam was profiled with and without the sample to properly calculate the S-Parameter (shown in Equation 7). Representative Z-scan data is shown as raw data with open and closed aperture data fits, which provide the n_2 and β results. The following figure gives an example of the Z-scan results.

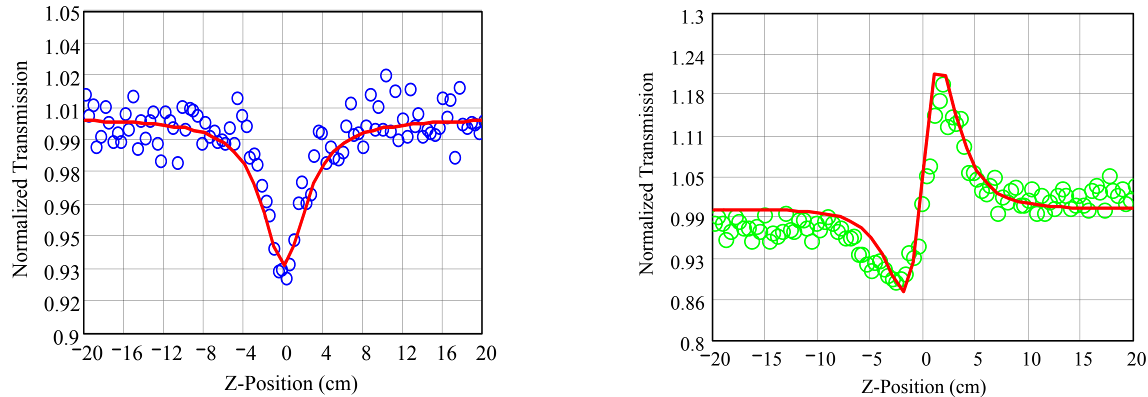

Figure 3 On the left is the normalized transmission for the open aperture and on the right is the normalized transmission for the closed aperture both for the SiC semi-insulating sample. The parameters used for this sample were energy of 3μJ, a 750mm lens, wavelength of 780nm, pulse width of 160fs, and a 5.1mm entrance aperture.

The results for the SiC and FS Z-scans are found in Table 3.

Table 3: Nonlinear measurements resulting from the Z-scan experiment using 780nm at 160fs; multiple energies were tested to provide a statistical average.

Sample	**β (cm/GW) Theory**	**β (cm/GW) Measured**	**n_2 (cm^2/GW) Theory**	**n_2 (cm^2/GW) Measured**
FS	NA	0	NA	2.60×10^{-7}
SiC semi-insulating	0.055	0.064	3.6×10^{-6}	4.75×10^{-6}
SiC conducting	0.055	0.052	3.6×10^{-6}	4.00×10^{-6}

From Table 3, the semi-insulating and conducting SiC nonlinear properties are relativity the same, which is not surprising since the dopant levels in the conducting sample are extremely small as stated earlier. The conductivity is electronic therefore it has no or little affect on the optical linear/nonlinear interactions, thus the nonlinear quantities are about the same. The SiC β and n_2 experimental results were compared to a simple two-parabolic-band model by Sheik-Bahae *et al* [16] for theoretically calculating the nonlinear absorption and index of refraction properties in

semiconductors. The bandgap used to calculate the theoretical β and n_2 was calculated using the wavelength at the 1% transmission point in the UV-Vis chart in Figure 4. This model was not used for FS since it is not a semiconductor.

The FS data results show a β = 0 cm/GW, and $n_2 = 2.6 \times 10^{-7}$ cm^2/GW. Referenced FS Z-scan results show similar n_2 values of 2.5×10^{-7} cm^2/GW [14], but published β values were not located primarily due to fact that FS has little or no nonlinear absorption (from its large bandgap). Since the FS n_2 experimental result is in good agreement with the published values the Z-scan experiment is in good working order and is ready to test the SiC samples. The SiC samples were tested and the results are given in Figure 3.

6. UV-Vis Study

A UV-Vis study was carried out to understand the linear transmission and to confirm the provided bandgap information shown in Table 2 using a Varian Cary 50 UV-Vis spectrometer. This device uses a Xenon flash lamp and monochromatic optics to send a beam of varying wavelengths (300nm to 900nm) through the sample to measure its transmission. The results for each SiC sample are given in the figure below.

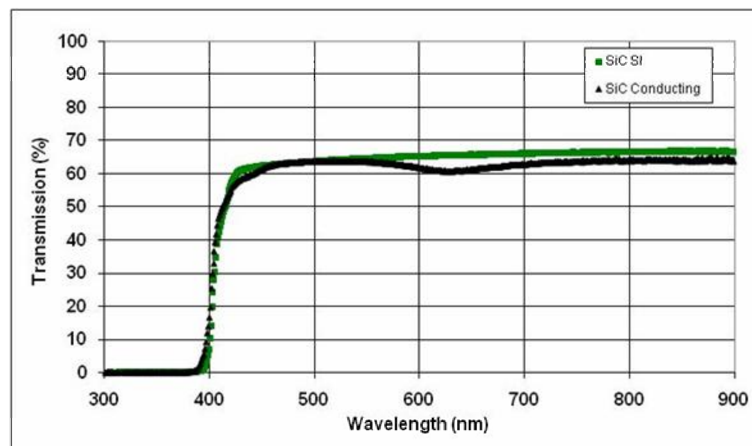

Figure 4 UV-Vis results on semi-insulating and conducting SiC.

From the UV-Vis results it demonstrates that both the semi-insulating and conducting SiC samples have a band edge at 400nm. Equation 12 below relates the cutoff wavelength of the SiC samples to the band gap in electron volts (eV).

$$\lambda = \frac{1239.8}{E(eV)}. \qquad \text{Equation 10}$$

Here, E is the energy with units of electron volts, λ is in units in nm, and Table 2 gives E = 3.1eV. Therefore, λ = 399.936 nm for both semi-insulating and conducting SiC, which is in agreement with the "turn on" wavelength in Figure 4. Furthermore, the conducting SiC sample has a dip centered at ~630nm that is consistent with multiple SiC conducting samples tested. The dip is may be due to the absorption of the Nitrogen dopant present in the conducting SiC sample. The transmissions are around 65% to 70% for each semi-insulating and conducting sample, which agrees with the DT results that show a nonlinear transmission at close to zero fluence.

7. Sample Characterization

The high NA line distribution processed into the SiC semi-insulating and conducting samples were further analyzed using optical microscopy and Atomic Force Microscopy (AFM) to understand the morphology of the index modified structures. The processed lines are on or just below the surface (~5μm to10μm), and the modifications form a hill/valley above/below the surface depending on the type of SiC processed. The figures below illustrate this effect. For these images, the optical microscope used is an Olympus upright digital BX51 microscope with Nomarski DIC capabilities that use high contrast prisms to produce increased contrast/resolution. This microscope also has measuring capabilities to ± 0.25μm or less, which is also traceable to NIST.

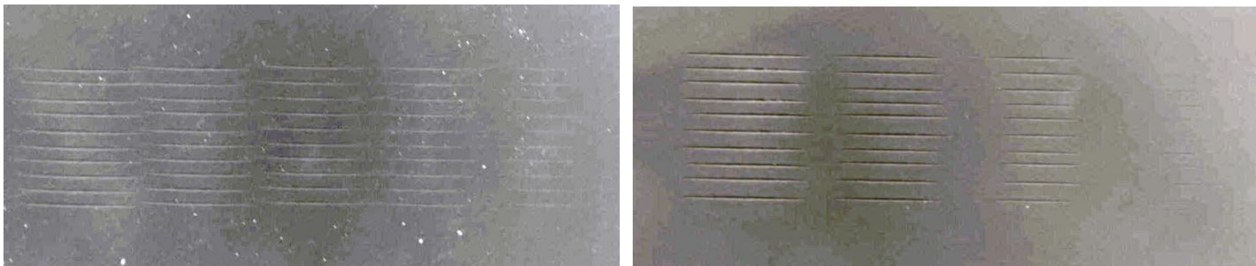

Figure 5 DT optical microscope results using Nomarski DIC and image processing for better viewing purposes for (left) semi-insulating SiC; (right) conducting SiC. Image processing was performed in order to better resolve the modified surface lines. These results were both done using 780nm at 160fs.

Here, the 2.5µm x 190µm *predicted* line spread is shown from the AFM to be ~5.5µm wide x 210µm long for the semi-insulating SiC and ~3.3µm wide x 193µm long for the conducting SiC sample. The difference in the predicted primarily comes from the sample makeup and the sample being at the exact focus as foreseen. The line spread (for semi-insulating and conducting both) decreases in both axes as the fluence/energy is decreased until the point where no visible damage occurs. The semi-insulating SiC sample results in more columns of modified lines which are due to it having a lower threshold than the conducting SiC sample. The processed lines, on both SiC types, were analyzed using the Nomarski DIC mode on the optical microscope (set in reflection mode). The semi-insulating SiC processed lines are more optically opaque, which may be caused from bulges or hills that form in the surface as observed in other types of bulk transparent dielectric substrates. AFM imaging will give a more precise measurement of the line spread morphology.

Atomic Force Microscopy (AFM) was performed using a Veeco Dimension 3100 with a Nanoscope 3a controller in tapping mode to evaluate the topography of line distributions fabricated just above the threshold. The height images were obtained from monitoring the cantilever oscillation amplitude during scanning. Figure 5 below shows some AFM results of a SiC semi-insulating sample with surface line modifications.

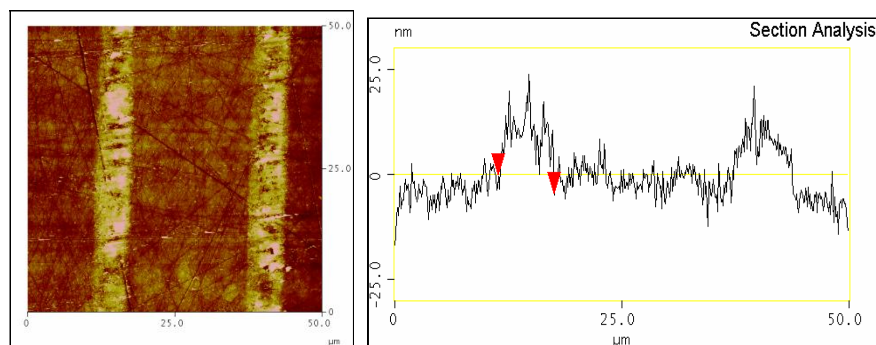

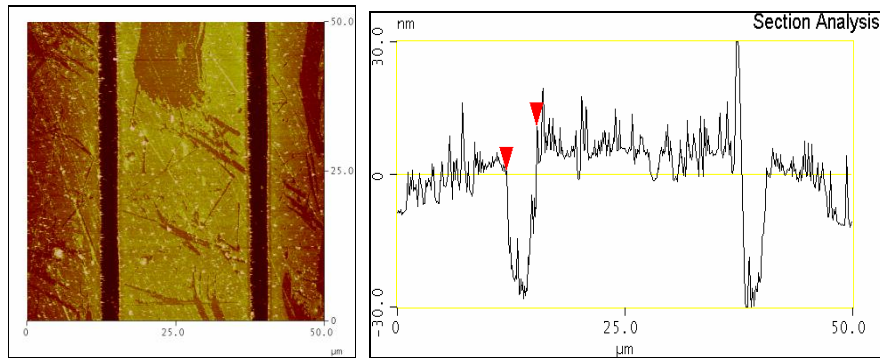

Figure 6 On the top shows AFM results of a 5.5µm wide and a 10nm raise surface modification on semi-insulating SiC material. On the bottom shows the conducting SiC sample AFM results of a 3.3µm wide and a 30nm trench surface modification.

The AFM results show a morphology of the line processed structures as being 3-5µm in width and about a 10-30nm hill or valley. The semi-insulating SiC sample forms lines protruding bulges that are raised by ~10nm and have a width of ~5.5µm. The conducting SiC sample forms line trenches that are ~30nm deep and have a width of ~3.3µm. The AFM concludes that the semi-insulating SiC surface modification by these line spreads creates a hill in the substrate surface, which may be due to a local subsurface restructuring has occurred or some other electronic trapping process [15] has forced the material to rise in the processed areas. Whereas, the conducting SiC sample forms trenches that may be due to surface structural damage caused by thermal breakdown of the molecular lattice to the inability for the crystal to dissipate heat, and/or oxidation and chemical reactions on the surface that give a different compound. The protruding lines in the semi-insulating sample also caused a broader line width instead of the predicted 2.5-3µm, and the valleys formed in the conducting samples create a sharper edge that results in a closer agreement to the predicted value. In any case, there is a morphology difference in the femtosecond laser processing of SiC between semi-insulating and conducting types. X-ray diffraction was performed on these SiC samples, but it was found that the damage areas were too small for the x-ray beam and only the bulk SiC was actually being measured – thus the x-ray diffraction tests were unsuccessful.

8. Conclusion

In this work we report important linear, nonlinear and femtosecond laser processing threshold properties that are useful to optical and material scientific communities. We concluded that there are only two observable differences between the two SiC types (even the samples visual appearance is similar), which are the UV-Vis absorption at ~630nm and the morphology after being femtosecond laser processed. The linear, nonlinear, and DT properties remain familiar to one another. The values of all the measured parameters vary within 20% of each other except for the high NA DT values which gives a 45% difference between semi-insulating and conducting types. Special thanks is given to AFRL personal Dr. Don Dorsey, Mr. Tom Kensky for providing the SiC samples, to Dr. Bill Mitchell for providing information on each of the SiC samples, to Dr. William Woody for help with the image processing, and to Dr. Angela Campbell for assisting with AFM results.

References and Links

1. G. Petite, P. Daguzan, S. Guizard, P. Martin, "Femtosecond History of Free Carriers in the Conduction Band of a Wide-Bandgap Oxide", IEEE Electrical Insulation and Dielectric Phenomena, 15, pgs 40-44 (1995).
2. A. Tien, S. Backus, H. Kapteyn, M. Murnane, G. Mourou, "Short-Pulse Laser Damage in Transparent Materials as a Function of Pulse Duration", University of Michigan, Physical Review Letters, pgs 3883 – 3886, (1999).
3. J. Copper, Purdue Wide Band Gap Semiconductor Device Research Program, http://www.ecn.purdue.edu/WBG/Index.html, Purdue University College of Engineering.
4. D., Molian, "Femtosecond Pulsed Laser Ablation of 3C-SiC Thin Film on Silicon", Appl. Phys. A, 839-846 (2003).
5. J. Ashcom, C. Schaffer, E. Mazur, "Numerical Aperture Dependence of Damage and White Light Generation from Femtosecond Laser Pulses in Bulk Fused Silica", J. Opt. Soc. Am. B, pgs 2317-2322, (2006).
6. Verdeyen, "Laser Electronics", Third Edition, Prentice Hall, Inc., pgs 50-55 (1995).
7. M. Lenzner, J. Kruger, S. Sartania, Z. Cheng, Ch. Spielmann, G. Mourou, W. Kautek, F. Krausz, "Femtosecond Optical Breakdown in Dielectrics", Physical Review Letters, pgs 4076-4079, (1998).
8. Strelstov, Ranka, Geata, "Femtosecond Ultraviolet Autocorrelation Measurements Based on Two-Photon Conductivity in Fused Silica", Optics Letters, Vol. 23, No. 10, pgs 798-800 (1998).
9. L. Shah, J. Tawney, M. Richardson, K. Richardson, "Self-Focusing During Femtosecound Micromachining of Silicate Glasses", IEEE Journal of Quantum Electronics, pgs 57-68, (2004).
10. A. Evwaraye, S. Smith, W. Mitchel, "Persistent photoconductance in n-type 6H-SiC", Journal of Applied Physics, pgs 4477-4481, (1995).
11. P. Chapple, J. Staromlynka, J. Herman, T. McKay, R. McDuff, "Single-Beam Z-scan: Measurement Techniques and Analysis", Journal of Nonlinear Optical Physics and Materials, pgs 251-293, (1997).
12. M. Sheik-Bahae, A. Said, T. Wei, D. Hagan, E. Van Stryland, "Sensitive Measurement of Optical Nonlinearities Using a Single Beam"; IEEE Journal of Quantum Electronics, pg s 760-769, (1990).
13. M. Yin, H. P. Li, S. H. Tang, W. Ji, "Determination of Nonlinear absorption and Refraction by Single Z-scan Method"; Appl. Phys. B, Vol. 70, pgs 587-591, (2000).
14. Yamane, Asahara, "Glasses for Photonics", Cambridge University Press , Pg. 174, (2000).
15. S. Mao, F. Quére, S. Guizard, X. Mao, R.Russo, G. Petite, P. Martin, "Dynamics of Femtosecond Laser Interactions with Dielectrics", Appl. Phys. A, 1695-1709, (2004).
16. M. Sheik-Bahae, D Hutchings, D. Hagan, E. Van Stryland, "Dispersion of Bound Electronic Nonlinear Refraction in Solids, IEEE Journal of Quantum Electronics, pgs 1296-1309, (1991).